Parameter Identification, Non-linearity, and Harmonic Effects in a Vernier Machine of the MAGNUS Type

Ali Mohammadi, Yaser Chulaee, Aaron M. Cramer[1], Ion Boldea[2], and Dan M. Ionel

SPARK Laboratory, Stanley and Karen Pigman College of Engineering, University of Kentucky, Lexington, KY, USA
[1]Stanley and Karen Pigman College of Engineering, University of Kentucky, Lexington, KY, USA
[2]Electrical Engineering Department, Polytechnic University of Timisoara, Timisoara, Romania

alimohammadi@uky.edu, yaser.chulaee@uky.edu, aaron.cramer@uky.edu,
ion.boldea@upt.ro, dan.ionel@ieee.org

***Abstract*— This paper discusses the parameter identification of MAGNUS, a dual-stator Vernier-type axial-flux machine. MAGNUS machine can operate with the minimum number of stator slots at an extremely high polarity and is designed with a spoke-type permanent magnet rotor which is capable of achieving a very high flux concentration ratio. The direct and quadrature axis inductances are obtained through multiple methods, and it is shown that despite having the spoke-type rotor, MAGNUS has a non-salient behavior. The paper also examines the effects of non-linearity and very high content of mechanical harmonics on the operation of the machine through finite element analysis (FEA). Results from the experimental tests on the MAGNUS prototype are used for validation of the analytical calculations and the 3-D FEA results.**

***Index Terms*—Parameter identification, Vernier machine, dual-stator, permanent magnet (PM) machine, d- and q-axis inductances, spoke rotor, high polarity, finite element analysis.**

I. Introduction

In recent years, there has been an increase in the research and development concerning high-performance machines, including those of axial-flux type [1]. Permanent magnet synchronous machines (PMSMs) with high specific torque and low speed have been previously studied in [2, 3]. An example of such a high-performance axial-flux Vernier-type machine is the dual-stator MAGNUS type, which was initially proposed and described in [4].

Vernier-type axial-flux machines use the Vernier effect. This effect involves having a different number of rotor and stator teeth or poles, resulting in a spatial phase difference between the rotor and stator magnetic fields. This phase difference enhances the machine's performance and efficiency. In Vernier-type axial-flux machines, the magnetic field lines move through the axial gap between the rotor and stator, creating a flux path that is parallel to the axis of rotation. This configuration allows for compact and lightweight designs while maintaining high torque density.

Using permanent magnet machines with high magnetic polarity in low-speed applications can improve torque density and efficiency due to a decrease in the amount of flux per pole associated with the stator winding. This results in the ability to employ smaller magnetic components and a reduction in the end turn volume. Vernier-type axial flux machines, have the potential to achieve a very high torque density and are promising candidates for low-speed direct drive and a variety of industrial and automotive applications.

Due to the unique design of these machines, they are often utilized in various applications such as electric vehicles, servo applications, and renewable energy systems such as wind turbine generators. They offer advantages such as high power density, improved efficiency, and a compact form factor, making them suitable for applications that require high torque, and low speed [5–7].

Vernier-type axial-flux machines have several advantages, such as having very few stator coils which can simplify the manufacturing of stator windings [8], and high rotor polarities that allow for magnetic flux concentration and higher torque density [9–11]. The power factor of these machines however is inherently low due to high magnetic leakage and a relatively large equivalent airgap [12]. In order to address this issue and improve the overall performance of these machines, dual stator arrangements have been suggested, e.g. MAGNUS machine in [13, 14].

This paper presents a systematic study of MAGNUS, a machine with 12 stator teeth and 40 rotor poles, which has a trade-off between the minimum number of stator coils and an ultra-high flux concentration versus having negligible reluctance torque. The direct and quadrature axis inductances are obtained through different methods demonstrating that despite its spoke-type rotor, MAGNUS indeed has a non-salient behavior. Further investigations are carried out on MAGNUS and since the stator slot opening is comparable to the rotor pole pitch, it results in a higher leakage inductance

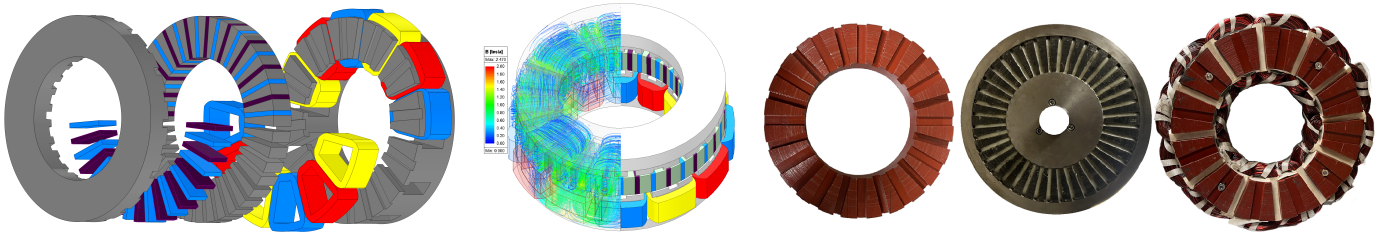

(a) (b) (c)

Fig. 1. MAGNUS topology; (a) Exploded view of the innovative construction with two stators only one with coils and a spoke-type rotor. (b) The 3-D FEA model shows the flux lines for half of the topology and the model in the other half. (c) The prototype components, namely the auxiliary stator, rotor with 40 PMs, and the main wound stator.

Table I
SPECIFICATIONS AND MAIN DIMENSIONAL PROPERTIES OF THE STUDIED THREE-PHASE 40-POLE DOUBLE-STATOR SINGLE-ROTOR VERNIER-TYPE AFPM MACHINE NAMED MAGNUS.

Parameter	Value	Unit
Rated power	3.5	hp
Rated speed	300	rpm
Airgap	1.5	mm
Rotor outer diameter	250	mm
Rotor inner diameter	150	mm
Rated copper losses	45	W
No. of rotor poles	40	–
No. of coils per phase	4	–
No. of turns per phase	104	–

due to the machine's extremely high polarity.

Additionally, FEA results are presented to demonstrate the non-linearity and mechanical harmonics in this machine. Only half of the machine structure was modeled using Ansys Electronics 2023 software [15], to reduce the computational burden [16]. The validity of the 3-D FEA simulations was assessed through analytical calculations and experimental testing of a prototype to ensure that it accurately reflects the specifications and operating conditions of the system under study.

II. MAGNUS TOPOLOGY AND OPERATING PRINCIPLE

MAGNUS is a dual-stator Vernier-type axial-flux machine that has a very high ratio of rotor poles to concentrated stator coils, where its topology is as shown in Fig. 1. The stator of this machine has 12 teeth, and each tooth includes two smaller auxiliary teeth that improve torque production. The rotor is designed with spoke-type permanent magnets, which provide high flux concentration and further increase the machine's torque density, which also allows for a smaller overall size and weight of the machine compared to traditional electric motors. The main specification of the machine under study is also reported in Table I.

This paper discusses the parameter identification of the MAGNUS including the resistances, self, mutual, d, and q-axis inductances, the effects of non-linearity, and the harmonic content in the airgap by using FEA results and experimental

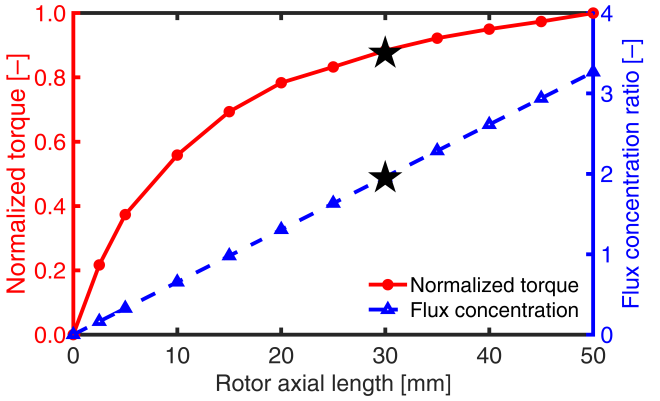

Fig. 2. Torque and the flux concentration ratio vs. rotor axial length at the rated loading. The machine has an extremely high flux concentration ratio at its design variable, which is shown with the ★.

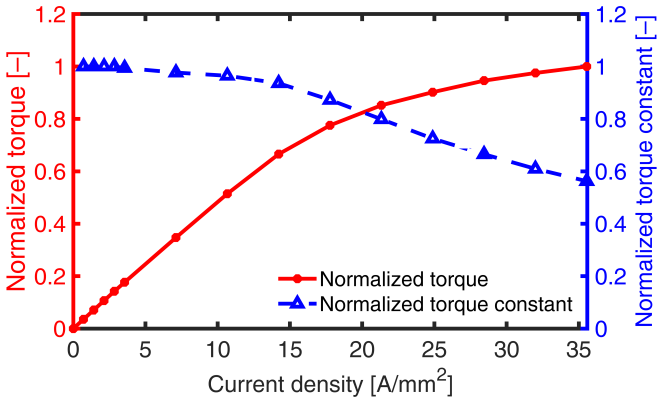

Fig. 3. Torque and torque constant vs. the current density, to show the effect of the non-linearity of MAGNUS as a result of the armature current. Torque and torque constant are normalized based on the peak torque at the maximum current density.

tests. MAGNUS uses double-sided stator coils that are concentrated around the main teeth that have notches at the tips which then create auxiliary teeth. This is combined with a very high polarity rotor with 40 PMs and is demonstrated in a single-rotor dual-stator axial flux configuration in Fig. 1.

The field modulation due to the Vernier effect not only reduces the rotor speed but also, enables the utilization of

varying numbers of pole pairs in both the rotor and the stator. MAGNUS has the exceptional capability of operating with a minimum number of 6 coils. This feature provides the potential for implementing novel cooling technologies, which many machines with a high number of stator teeth can not achieve. This attribute of MAGNUS, to use innovative cooling technologies, makes it suitable for a wide range of applications. MAGNUS can use varying numbers of stator teeth and rotor poles.

The operational principle of the MAGNUS machine involves modulating the armature magneto motive force (MMF) to generate a flux density component in the air gap that corresponds to the poles of the rotor. This modulation is achieved by utilizing main and auxiliary stator teeth and slots with a different number of poles compared to the rotor. The specific relationship between the number of rotor poles, main and auxiliary stator teeth, and armature poles are established as:

$$P_r = 2 \times T_{ms} \times t_{st} - P_a, \tag{1}$$

where, P_r refers to the number of rotor poles which in MAGNUS it is equal to 40, T_{ms} the number of main stator teeth which here is 12, t_{st} the number of auxiliary stator teeth which is 2, and P_a the number of armature poles which is 8 in this machine.

III. Effect of Non-linearity and Harmonics

The operation of this machine is accompanied by the occurrence of non-linearity, which arises from two contributing factors. Firstly, the effect of the excitation field, in which the permanent magnets create the magnetic field within the machine, and secondly, the influence of the armature reaction, which is the magnetic field produced by the armature current of the machine.

One of the most distinctive characteristics of this machine is the spoke-type rotor, which has a profound impact on the concentration of flux within the machine, as illustrated in Fig. 2. By considering h_{PM} as the length of the PM in the axial direction, the flux concentration ratio ξ is calculated as:

$$\frac{h_{PM}}{\tau_p}, \tag{2}$$

where, τ_p is the rotor pole pitch, i.e., rotor outer circumference πD_s divided by the number of PMs n_{PM}. The flux concentration effect due to the spoke-type arrangement employed in the MAGNUS is particularly beneficial because of the very high number of poles as the magnetic flux of two magnets, contributes to the airgap magnetic flux in each pole.

MAGNUS has an extremely high ratio of rotor polarity to stator teeth number. This high number of rotor pole to stator teeth ratio is designed to maximize the MAGNUS flux concentration ratio. The normalized torque and flux concentration ratio are derived as functions of rotor height and shown in Fig. 2. The normalized torque is linear, up to a rotor height of 5mm, and exhibits saturation beyond this point. These

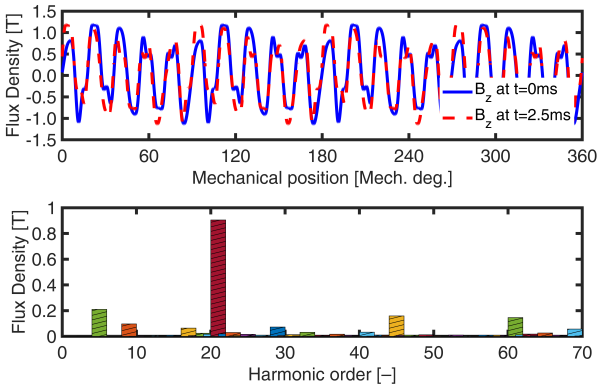

Fig. 4. The axial component of the magnetic flux density in the airgap between the active stator and rotor at the median diameter, having a very high harmonic content.

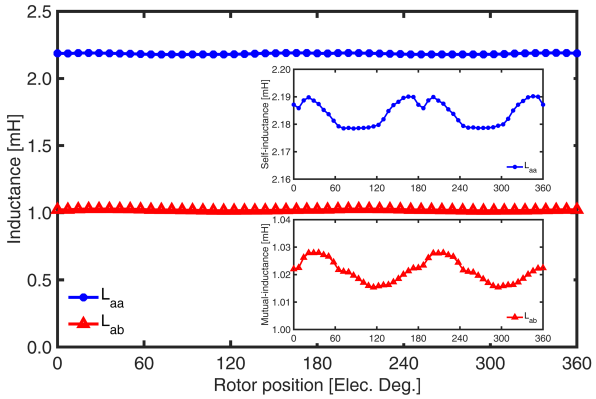

Fig. 5. Self and mutual inductances of the MAGNUS machine demonstrate a very small variation over one electrical period. Zoomed-in views are provided to illustrate the small variation.

results demonstrate the effectiveness of the MAGNUS machine's design in achieving ultra-high flux concentration and highlight its superior performance. The non-linear behavior in the MAGNUS machine is not only due to the effect of the excitation field but also to the influence of the armature excitation which is the effect of the armature current on the magnetic field produced by the permanent magnets in the machine. This effect is particularly pronounced in machines with high current levels, leading to non-linear behavior.

The non-linear behavior and saturation can be observed in the normalized torque and torque constant curves as shown in Fig. 3. The curve of normalized torque shows the effect of non-linearity and saturation when the current density exceeds 15A/mm^2. This effect is also reflected in the normalized torque constant curve.

In this machine, because of the very high polarity, the slot opening is comparable to the rotor pole pitch, which results in a higher leakage inductance. The waveform of the magnetic flux density distribution in the airgap in the axial direction between the active stator and rotor is depicted in Fig. 4. The harmonic spectrum of the flux density distribution, including

the high distortion caused by the significant mechanical harmonics content, is also depicted in Fig. 4.

IV. DQ Axis Inductances and Discussion on Saliency

The direct and quadrature axis inductances have a significant impact on the torque-producing ability and flux control of permanent magnet synchronous machines [17]. These inductances also affect the efficiency and power factor of the machine and are essential for creating mathematical models of electrical machines, which makes the precise calculation and understanding of these inductances a necessity for analyzing their behavior. There are different methods to calculate the values of d- and q-axis inductances. The induced voltage V in a permanent magnet machine can be related to the back-EMF $\omega\lambda_{pm}$ and machine parameters, including the winding resistance R_s, the inductance of the direct axis L_d and quadrature axis L_q, and the direct and quadrature axis currents I_d, I_q. This relation is given by:

$$V_d = R_s I_d - \omega L_q I_q, \tag{3}$$

$$V_q = R_s I_q + \omega\lambda_{pm} + \omega L_d I_d, \tag{4}$$

$$V = V_d + jV_q, \tag{5}$$

that is derived from the phasor diagram of PM machines. Here the current of the motor is given as:

$$I = I_d + jI_q. \tag{6}$$

By using 3-D FEA the values of induced voltage, back-EMF, and phase current and their phases can be obtained. Applying the current in the d- and q-axis respectively, the aforementioned equation gives the reactance of the d- and q-axis, therefore the corresponding inductances can be obtained.

The second method used in the calculation of the inductances involves the Park transformation (P_T). In this method, the self (e.g. L_{aa}) and mutual (e.g. L_{ab}) inductances of the three-phase windings are obtained from the 3D FEA and by conducting a Fourier analysis of these inductance profiles; expressions for self and mutual inductances in this form can be obtained respectively by:

$$\begin{cases} L_{aa}(\theta) = L_{sa} + L_{sv}\cos(2\theta) \\ L_{bb}(\theta) = L_{sa} + L_{sv}\cos(2\theta - 4\pi/3) \\ L_{cc}(\theta) = L_{sa} + L_{sv}\cos(2\theta - 2\pi/3) \\ L_{ab}(\theta) = -L_{ma} + L_{mv}\cos(2\theta - 2\pi/3) \\ L_{bc}(\theta) = -L_{ma} + L_{mv}\cos(2\theta) \\ L_{ca}(\theta) = -L_{ma} + L_{mv}\cos(2\theta - 4\pi/3) \end{cases}, \tag{7}$$

and these inductances are depicted in Fig. 5, respectively. By defining L_{abc} as a matrix of these inductances the d- and q-axis inductances can be calculated by:

$$L_{dq0} = P_T L_{abc} {P_T}^{-1}. \tag{8}$$

The values for d- and q-axis inductances using the first method are 3.20mH and 3.12mH, and using the second method

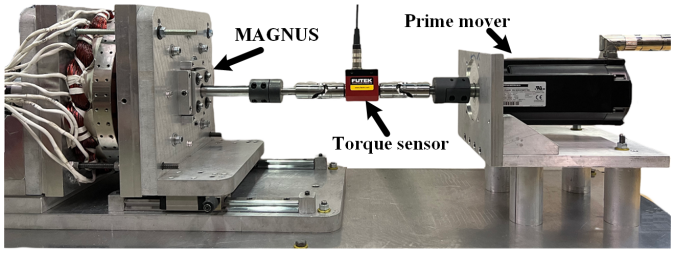

Fig. 6. Test fixture for static torque versus current and phase back-EMF measurements of the MAGNUS machine, which includes a servo motor as an electromagnetic break on the right-hand side and a torque sensor in the middle of the shaft couplings.

Table II
THE INDUCTANCE AND RESISTANCE WERE EVALUATED THROUGH EXPERIMENTAL TESTS AND FEA AT $I_d = 0$ AND A FREQUENCY OF 100HZ, WHICH IS THE DESIGNATED OPERATING FREQUENCY FOR THE MACHINE.

Parameter	Unit	FEA	Test	Difference
L_{aa}	[mH]	2.18	2.02	7.3%
L_{bb}	[mH]	2.18	2.00	8.2%
L_{cc}	[mH]	2.18	1.95	10.6%
L_{mutual}	[mH]	1.02	0.90	11.4%
R_{phase}	[Ω]	0.170	0.175	3.0%

are 3.19mH and 3.21mH, respectively. The difference in the results of these methods for d- and q-axis inductance values are 0.3% for the former and 2.8% for the latter. The results show that in this machine the d- and q-axis inductances are almost equal, which indicates that according to:

$$T_e = \frac{3}{2}\frac{P}{2}\left[\lambda_{pm} i_q + \left(L_d - L_q\right) i_d i_q\right], \tag{9}$$

the reluctance component of the torque is negligible. The analytically calculated torque and voltage curves using the calculated d- and q-axis inductances and the torque and voltage curves obtained from the 3-D FEA model for MAGNUS are depicted in Fig. 7, which shows a close agreement between the

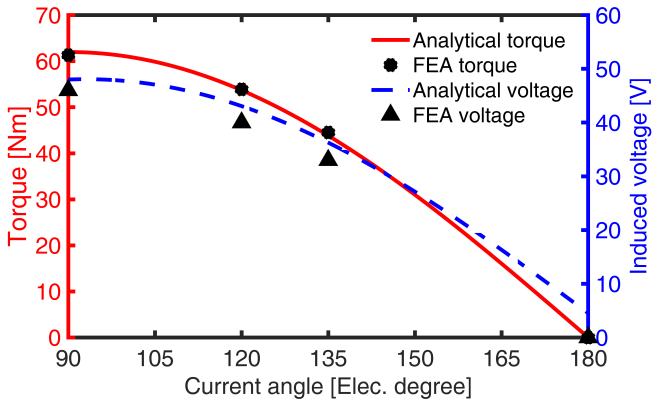

Fig. 7. The lack of saliency and hence no reluctance torque are demonstrated by calculating the MAGNUS electromagnetic torque and induced voltage analytically and with 3-D FEA.

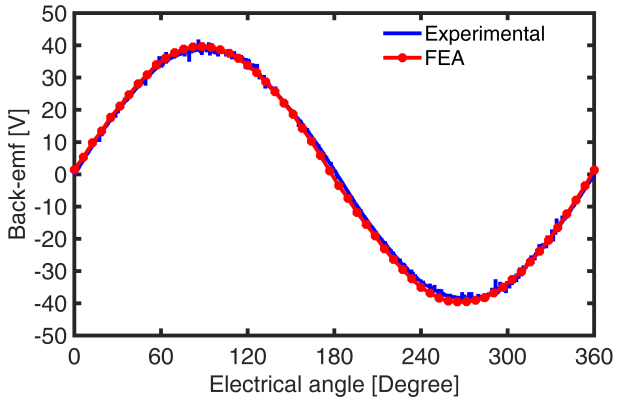

Fig. 8. Experimental and 3-D FEA results for phase voltage of the MAGNUS prototype. The phase voltage values are shown for one electric period and for the rotor speed of 100rpm, which demonstrates a very good agreement between the measurement and simulation.

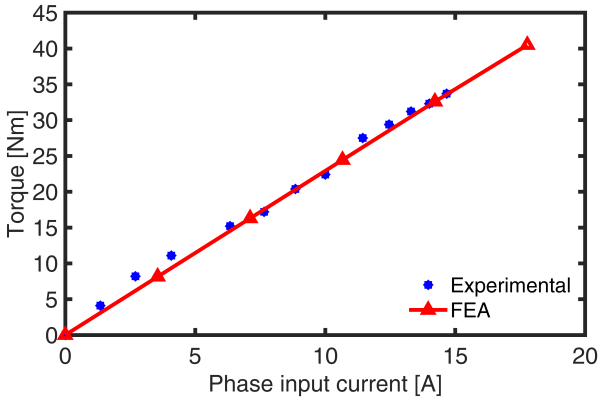

Fig. 9. Experimental and 3-D FEA results for the static torque of the MAGNUS prototype. The three-phase windings are connected in a star configuration. Each phase has 4 coils in series. DC current is applied to the windings in the experimental tests, where the value of the applied DC current is equal to the peak of the AC current applied in simulations.

results and confirms the accuracy of the analytical calculations.

V. Experimental Results and Discussion

The prototype for the MAGNUS has been fabricated and it is shown in Fig. 6. The machine performance is evaluated by performing several experimental tests and comparing the results to the 3-D FEA simulations. The prototype has been tested in open circuit condition and the back-EMF for one phase is shown in Fig. 8. The results of static torque measurements are shown in Fig. 9.

The experimental results obtained in this study on the machine back-EMF and static torque are consistent with the simulations performed, providing strong evidence that the theoretical model accurately represents the prototype.

Furthermore, Table II summarizes the experimental and simulation results for self and mutual inductances of MAGNUS, where the inductance and resistance were evaluated at $I_d = 0$ and a frequency of 100Hz, which is the designated operating frequency for the machine. The experimental results are in good agreement with the simulation results, and the difference between the simulation results and measurements is shown.

VI. Conclusion

This study primarily investigated the parameters of the dual-stator single-rotor MAGNUS machine and examined the impact of non-linearity on its performance. The study showed that due to the MAGNUS machine, characterized by its high pole count, spoke-type rotor, and minimal stator teeth number, can achieve an ultra-high flux concentration ratio, resulting in a high airgap magnetic flux density.

Despite the spoke-type rotor, in MAGNUS the d- and q-axis inductances are nearly equal, which is good for operation with $I_d = 0$ for maximum torque per ampere (MTPA), therefore the trade-off in having such a high flux concentration is virtually no reluctance torque. Additionally, the study explored the harmonic content of the magnetic flux density in the airgap. Different methods were used to calculate the d- and q-axis inductances and to further validate the accuracy of calculations, the results were compared to 3-D FEA simulations. Finally, the experimental results of the open circuit test, static torque measurements, and self and mutual inductance measurements were found to be in good agreement with the simulation of the model.

Acknowledgment

This paper is based upon work supported by the National Science Foundation (NSF) under Award No. #1809876. Any opinions, findings, conclusions, or recommendations expressed in this material are those of the authors and do not necessarily reflect the views of the NSF. The support of Ansys Inc., and University of Kentucky, the L. Stanley Pigman Chair in Power endowment is also gratefully acknowledged.

References

[1] F. Nishanth, J. Van Verdeghem, and E. L. Severson, "A review of axial flux permanent magnet machine technology," *IEEE Transactions on Industry Applications*, vol. 59, no. 4, pp. 3920–3933, 2023.

[2] V. Rallabandi, P. Han, M. G. Kesgin, N. Taran, and D. M. Ionel, "Axial-field Vernier-type flux modulation machines for low-speed direct-drive applications," in *2019 IEEE Energy Conversion Congress and Exposition (ECCE)*, 2019, pp. 3123–3128.

[3] A. Mohammadi and S. M. Mirimani, "Design and analysis of a novel permanent magnet assisted synchronous reluctance machine using finite-element-method," in *2020 11th Power Electronics, Drive Systems, and Technologies Conference (PEDSTC)*, 2020, pp. 1–5.

[4] M. G. Kesgin, P. Han, N. Taran, and D. M. Ionel, "Optimal study of a high specific torque Vernier-type axial-flux PM machine with two different stators and a single winding," in *IEEE ECCE*, 2020, pp. 4064–4067.

[5] L. Xu, Z. Sun, W. Zhao, B. Liu, K. Du, and G. Liu, "Design and evaluation of linear primary permanent magnet Vernier machines for urban railway transportation," *IEEE Transactions on Industry Applications*, vol. 59, no. 2, pp. 1678–1688, 2023.

[6] R. Li, C. Shi, R. Qu, D. Li, X. Ren, V. Fedida, and Y. Zhou, "A novel modular stator fractional pole-pair permanent-magnet Vernier machine with low torque ripple for servo applications," *IEEE Transactions on Magnetics*, vol. 57, no. 2, pp. 1–6, 2021.

[7] B. Kim, "Design of a direct drive permanent magnet Vernier generator for a wind turbine system," in *2018 IEEE Energy Conversion Congress and Exposition (ECCE)*, 2018, pp. 4275–4282.

[8] A. Mohammadi, Y. Chulaee, C. Aaron, I. Boldea, and D. M. Ionel, "Axial flux permanent magnet Vernier machine with single-wound dual-stator and spoke permanent magnet rotor for electric vehicle in-wheel traction," in *2023 IEEE Transportation Electrification Conference & Expo (ITEC)*, 2023.

[9] L. Fang, D. Li, and R. Qu, "Torque improvement of Vernier permanent magnet machine with larger rotor pole pairs than stator teeth number," *IEEE Transactions on Industrial Electronics*, pp. 1–11, 2023.

[10] A. W. Bandarkar, Y. Sozer, and M. K. Mahmud Bin Azam, "Performance analysis of slotless dual-stator and single-rotor axial-flux permanent magnet machine," in *IEEE ECCE*, 2022, pp. 1–7.

[11] A. Mohammadi, O. A. Badewa, Y. Chulaee, D. M. Ionel, S. Essakiappan, and M. Manjrekar, "Direct-drive wind generator concept with non-rare-earth PM flux intensifying stator and reluctance outer rotor," in *2022 11th International Conference on Renewable Energy Research and Application (ICRERA)*, 2022, pp. 582–587.

[12] D. Li, R. Qu, and T. Lipo, "High power factor Vernier permanent magnet machines," in *2013 IEEE Energy Conversion Congress and Exposition*, 2013, pp. 1534–1540.

[13] M. G. Kesgin, P. Han, D. Lawhorn, and D. M. Ionel, "Analysis of torque production in axial-flux Vernier PM machines of the MAGNUS type," in *2021 IEEE International Electric Machines & Drives Conference (IEMDC)*, 2021, pp. 1–5.

[14] V. Rallabandi, N. Taran, D. M. Ionel, and I. G. Boldea, "MAGNUS — an ultra-high specific torque PM axial flux type motor with flux focusing and modulation," in *2017 IEEE Energy Conversion Congress and Exposition (ECCE)*, 2017, pp. 1234–1239.

[15] *Ansys® Electronics Desktop, Maxwell, version 23.1, 2023, ANSYS Inc.*

[16] M. Rosu, P. Zhou, D. Lin, D. M. Ionel, M. Popescu, F. Blaabjerg, V. Rallabandi, and D. Staton, *Multiphysics simulation by design for electrical machines, power electronics and drives*. John Wiley & Sons, 2017.

[17] D. Ionel, M. Balchin, J. Eastham, and E. Demeter, "Finite element analysis of brushless dc motors for flux weakening operation," *IEEE Transactions on Magnetics*, vol. 32, no. 5, pp. 5040–5042, 1996.